THE JOURNAL OF BIOLOGICAL CHEMISTRY VOL. 282, NO. 33, pp. 23818–23828, August 17, 2007

Accelerating Amyloid-β Fibrillization Reduces Oligomer Levels and Functional Deficits in Alzheimer Disease Mouse Models*[S]

Received for publication, February 5, 2007, and in revised form, May 30, 2007 Published, JBC Papers in Press, June 4, 2007, DOI 10.1074/jbc.M701078200

Irene H. Cheng[‡§], Kimberly Scearce-Levie[‡§], Justin Legleiter[‡§], Jorge J. Palop[‡§], Hilary Gerstein[‡], Nga Bien-Ly[‡], Jukka Puoliväli[‡§1], Sylvain Lesné[¶], Karen H. Ashe[¶], Paul J. Muchowski[‡§‖], and Lennart Mucke[‡§2]

From the [‡]Gladstone Institute of Neurological Disease, San Francisco, California 94158, the Departments of [§]Neurology and [‖]Biochemistry and Biophysics, University of California, San Francisco, California 94143, and the [¶]Department of Neurology, University of Minnesota Medical School, Minneapolis, Minnesota 55455

Many proteins suspected of causing neurodegenerative diseases exist in diverse assembly states. For most, it is unclear whether shifts from one state to another would be helpful or harmful. We used mutagenesis to change the assembly state of Alzheimer disease (AD)-associated amyloid-β (Aβ) peptides. *In vitro*, the "Arctic" mutation (AβE22G) accelerated Aβ fibrillization but decreased the abundance of nonfibrillar Aβ assemblies, compared with wild-type Aβ. In human amyloid precursor protein (hAPP) transgenic mice carrying mutations adjacent to Aβ that increase Aβ production, addition of the Arctic mutation markedly enhanced the formation of neuritic amyloid plaques but reduced the relative abundance of a specific nonfibrillar Aβ assembly (Aβ*56). Mice overexpressing Arctic mutant or wild-type Aβ had similar behavioral and neuronal deficits when they were matched for Aβ*56 levels but had vastly different plaque loads. Thus, Aβ*56 is a likelier determinant of functional deficits in hAPP mice than fibrillar Aβ deposits. Therapeutic interventions that reduce Aβ fibrils at the cost of augmenting nonfibrillar Aβ assemblies could be harmful.

Alzheimer disease (AD)[3] and many other neurodegenerative disorders are associated with the accumulation of abnormal protein assemblies in the central nervous system (CNS). Much evidence suggests that this association reflects a causal relationship in which the abnormal proteins actually trigger the neuronal dysfunction and degeneration that characterize these conditions (1–3). The prevalence of AD and other neurodegenerative proteinopathies is increasing rapidly around the world, most likely because of their age dependence, the increasing longevity of many populations, and the lack of effective strategies for treatment and prevention (4–6). This alarming trend underlines the need to better understand the relationship between the accumulation of abnormal proteins in the CNS and the decline of neurological function.

This relationship has been difficult to analyze in depth because proteins associated with neurodegenerative disorders can exist in diverse assembly states, and distinct assemblies can differ markedly in pathogenic potential. For example, the amyloid-β (Aβ) peptide, which seems to play a causal role in AD, can exist as monomers, low molecular weight oligomers (such as dimers and trimers), larger globular oligomers (such as Aβ*56, Aβ-derived diffusible ligands, amylospheroids, and globulomers), amyloid pores, protofibrils, fibrils, and amyloid plaques that contain densely packed Aβ fibrils and a large number of other molecules and cellular elements (7–15). Which of these structures contributes most critically to neurological decline in AD is a matter of active study and debate that has important implications for therapeutic interventions. Studies of transgenic mice with neuronal expression of human amyloid precursor proteins (hAPP), from which Aβ is released by proteolytic cleavage, suggest that nonfibrillar Aβ assemblies are more critical than amyloid plaques in the pathogenesis of AD-related neuronal dysfunction and memory deficits (15–20). However, there also is evidence for a pathogenic role of plaques and plaque-associated neuritic dystrophy (21–24).

Shifting Aβ from one assembly state to another may have profound effects on the pathogenesis of AD. Such shifts can result from genetic alterations and pharmacological interventions that change the amino acid composition of Aβ. For example, increasing the abundance of Aβ1–42 relative to shorter Aβ species promotes aggregation of Aβ monomers and plaque formation (25), whereas increasing the relative abundance of Aβ1–40 appears to counteract these processes (18, 26, 27). Mutations within the Aβ sequence that cause AD or related conditions also have marked effects on the assembly of Aβ (28).

The current study focuses on a familial AD-linked point mutation within Aβ (E22G, "Arctic mutation") that accelerates the aggregation of Aβ into protofibrils and fibrils *in vitro* (29–33). We investigated by atomic force microscopy (AFM) how

* This work was supported in part by National Institutes of Health Grants AG011385, AG022074, and AG023501 (to L. M.), NS33249 (to K. H. A.), and a Facilities Grant (RR 18928-01) from the National Institutes of Health National Center for Research Resources. The costs of publication of this article were defrayed in part by the payment of page charges. This article must therefore be hereby marked "*advertisement*" in accordance with 18 U.S.C. Section 1734 solely to indicate this fact.

[S] The on-line version of this article (available at http://www.jbc.org) contains supplemental Table S1, Figs. S1–S4, and Movies S1 and S2.

[1] Present address: Cerebricon Ltd., 70211 Kuopio, Finland.

[2] To whom correspondence should be addressed: 1650 Owens St., San Francisco, CA 94158. Tel.: 415-734-2504; Fax: 415-355-0131; E-mail: lmucke@gladstone.ucsf.edu.

[3] The abbreviations used are: AD, Alzheimer disease; Aβ, amyloid-β; hAPP, human amyloid precursor protein; CNS, central nervous system; AFM, atomic force microscopy; NTG, nontransgenic; TG, transgenic; β-CTF, β-secretase-generated C-terminal APP fragment; Tricine, *N*-[2-hydroxy-1,1-bis(hydroxymethyl)ethyl]glycine; ANOVA, analysis of variance; GuHCl, guanidine hydrochloride.

the Arctic mutation affects the balance between fibrillar and nonfibrillar Aβ assemblies in cell-free conditions and compared its effect on the relative abundance of neuritic amyloid plaques and nonfibrillar Aβ assemblies in brain tissues of hAPP mice. Lastly, we examined whether behavioral deficits and depletions of synaptic activity-related proteins in these mice relate more closely to plaques or nonfibrillar Aβ assemblies.

EXPERIMENTAL PROCEDURES

Ex Situ AFM—Wild-type (wt) and Arctic mutant synthetic Aβ1–42 (Biopeptide, San Diego, CA) were dissolved in 100% 1,1,1,3,3,3-hexafluoro-2-propanol (HFIP; Sigma) to 0.5 mg/ml and dried under vacuum. The HFIP-treated peptides were resuspended to 5 mg/ml in anhydrous dimethyl sulfoxide and incubated for 1 h at 37 °C. This stock solution was diluted in phosphate-buffered saline to a final concentration of 100 μg/ml and agitated at 1000 rpm at 37 °C. An aliquot from each sample was taken at various time intervals for immediate deposition. Aβ*56 was purified from forebrains of Tg2576 mice by immunoaffinity chromatography followed by size-exclusion chromatography as described (15). Three 5-μl samples of each incubation solution were deposited on freshly cleaved mica (SPI, West Chester, PA) and allowed to sit for 30 s. The substrate was washed twice with 100 μl of ultra-pure water, and the sample was then dried under a gentle stream of air. Tapping-mode AFM in air was performed with a Nanoscope IIIa system (Veeco, Santa Barbara, CA) equipped with a vertical-engage E scanner. Standard etched silicon probes (nominal spring constant, 50 N/m; resonance frequency, 300 kHz) were used. Typically, the following imaging parameters were used: drive amplitude of 150–500 kHz with set points of 0.8–1.0 V, scan frequencies of 4–5 Hz, image resolution of 512 by 512 points, and scan sizes of 3–12 μm. Custom software was used for AFM image analysis (35). Volume measurements were corrected for lateral tip contributions as described (36). For image quantification, nonfibrillar Aβ assemblies (oligomers and protofibrils) were defined as any structure with a height of 1–6 nm and a width to length (aspect) ratio smaller than 2.5. Fibrillar Aβ assemblies (fibrils and larger aggregates) were defined as any structure with a height larger than 6 nm and an aspect ratio of 2.5 or above. The ratio of nonfibrillar to fibrillar Aβ in Fig. 1*D* was calculated from the percent area occupied by each type of Aβ assembly as defined above.

In Situ AFM—*In situ* AFM experiments were performed with a Nanoscope IIIa MultiMode scanning probe microscope equipped with a fluid cell and a vertical engage E-scanner. Images were taken with a V-shaped oxide-sharpened silicon nitride cantilever with a nominal spring constant of 0.5 N/m. Scan rates were set at 1–3 Hz with cantilever drive frequencies of ~8–10 kHz. Freshly cleaved mica substrates were used, and phosphate-buffered saline was added to the cell in 35-μl aliquots by the hanging-drop method. Once the cantilever had successfully engaged the surface, a 15-μl aliquot of freshly made 1000 μg/ml Aβ-Wt or Aβ-Arctic was injected into the fluid cell, resulting in a final concentration of 300 μg/ml.

Experimental Animals—Artic-mutant hAPP (ARC) lines were generated in C57BL/6N mice (Harlan, Indianapolis, IN) and crossed onto the C57BL/6J background (Jackson Laboratory, Bar Harbor, ME) for 6–8 generations (34). The J20 line was generated in C57BL/6 x DBA/2 hybrids (18) and crossed onto the C57BL/6J background for more than 10 generations. Most results were compared with results in nontransgenic (NTG) littermates from each line to control for any line-specific effects. Unless indicated otherwise, mice were analyzed at 3–4 months of age. The studies were approved by the Institutional Animal Care and Use Committee of the University of California, San Francisco, and conducted in compliance with the National Institutes of Health's "Guide for the Care and Use of Laboratory Animals."

Behavioral Tests—Two independent, genotype- and line-balanced cohorts of singly housed male mice and NTG littermate controls from lines J20, ARC6, and ARC48 ($n = 9–13$/group) were tested in the sequence of elevated plus maze, open field, Y maze, and Morris water maze. The experimenter was blind to line and genotype during testing.

Open Field—Activity in the open field was tested with the automated Flex-Field/Open Field Photobeam Activity System (San Diego Instruments, San Diego, CA). The system consisted of two identical clear plastic chambers (41 × 41 × 38 cm), a PAS control box, a PC interface board, and a microcomputer for recording and analysis of data. Two sensor frames, each consisting of a 16 × 16 photobeam array at 1.5 cm and 6 cm above the bottom of the cage, were used to detect movements in the horizontal and vertical planes. The test was initiated by placing the mouse in the center of the arena. Horizontal beam breaks (ambulatory moves) in the arena were counted over 15 min. The arena was cleaned and dried after each test.

Y-Maze—The Y-maze was constructed of black plastic walls (10 cm high). It consisted of three compartments (10 cm × 10 cm) connected with 4 cm × 5 cm passages. The mouse was placed in one of the compartments and allowed to move freely for 6 min. An arm entry was manually recorded when all four paws entered the compartment. After each test, the maze was thoroughly cleaned.

Elevated Plus Maze—The elevated plus-shaped maze consisted of two open arms and two closed arms equipped with rows of infrared photobeams (Hamilton-Kinder, Poway, CA). Mice were habituated to dim lighting in the testing room for 30 min and then were placed individually at the center of the apparatus and allowed to explore for 10 min. The time spent and distance traveled in each of the arms were recorded by infrared beam breaks. After each mouse was tested, the apparatus was thoroughly cleaned.

Morris Water Maze—The water maze consisted of a pool (122 cm in diameter) containing opaque water (18 °C) and a platform (14 cm in diameter) submerged 1.5 cm under the water. For cued training sessions (days 1–3), the platform was marked with a visible beacon, and the mice were trained to locate the platform over six sessions (two per day, 4 h apart) each with two trials. The platform location was changed for each session. Hidden platform training (days 4–8) consisted of 10 sessions (two per day, 4 h apart), each with three trials. The platform location remained constant in the hidden platform sessions, and the entry points were changed semirandomly between trials. The maximum trial time was 60 s. Mice that failed to find the platform were led to it and placed on it for 15 s.

A day after the last hidden platform training session, a probe trial was conducted by removing the platform and allowing mice to search in the pool for 1 min. Time to reach the platform, time in target quadrant, platform crossings, path length, and swim speed were recorded with an EthoVision video tracking system (Noldus, Netherlands).

Immunoblotting and Immunohistochemistry—Mice were sacrificed 2 days after behavioral testing, and their brains were cut in half sagittally. One half was fixed for 48 h in 4% paraformaldehyde for immunohistochemical analysis, and the other was frozen in dry ice for biochemical analysis. To measure total Aβ1-x and Aβ1–42, snap-frozen forebrains were homogenized in 5 M guanidine buffer, and human Aβ peptides were quantitated by ELISA as described (18). Protein fractionation and Aβ*56 detection in hAPP mice were performed as described (15). Briefly, total proteins (100 μg) from the radioimmune precipitation assay buffer (RIPA) soluble fraction were separated on 10.5–20% Tricine gels or 4–12% Bis-Tris gels and transferred to nitrocellulose membrane (0.2 μm pore size, Bio-Rad). Biotinylated 6E10 antibody (1:1000, Signet, Dedham, MA) and ExtrAvidin (1:5000, Sigma) were used for Western blotting. Immunohistochemistry was performed as described (20) on floating 30-μm sliding microtome sections with anti-Aβ (3D6, 1:500, Elan Pharmaceuticals, South San Francisco, CA), anti-APP (8E5, 1:1000, Elan Pharmaceuticals), anti-Fos (Ab-5, 1:10,000, Calbiochem) or anti-calbindin (1:15,000; Swant, Bellinzona, Switzerland) antibodies. Diaminobenzidine was used as the chromagen. Images were acquired with a digital camera (Axiocam, Carl Zeiss). Densitometric quantification of calbindin immunoreactivity was performed with Bioquant (20). For double-labeling of amyloid plaques and dystrophic neurites, floating sections were stained with monoclonal anti-hAPP antibody (8E5, 1:1000, Elan Pharmaceuticals), mounted on glass slides, and stained with 0.015% thioflavin-S. Images were collected with a confocal microscope (Bio-Rad).

Statistical Analysis—Statistical analyses were performed with SPSS11 (SPSS, Chicago, IL) or Statview (SAS Institute, Cary, NC). Quantitative data are reported as mean ± S.E. Pairs of means were compared by unpaired two-tailed *t* test and multiple means by ANOVA and Tukey-Kramer posthoc test. Learning curves in the water maze were analyzed by repeated-measures ANOVA. Differences in survival curves were assessed by Kaplan-Meier analysis. Correlations were examined by simple regression analysis.

RESULTS

The Arctic Mutation Markedly Increases the Ratio of Fibrillar to Nonfibrillar Aβ in Vitro—Whereas it is well established that Aβ-Arctic aggregates more quickly than Aβ-Wt (29, 32), the specific aggregates formed and their ratios have, to our knowledge, not yet been analyzed by AFM. This technique provides quantitative three-dimensional morphological information unavailable with other approaches, such as analytical ultracentrifugation or dye-binding experiments. We first used *in situ* AFM to monitor the early events of synthetic Aβ1–42 assembly in real time under cell-free conditions as described (45).

At a solution concentration of 62.5 μM, Aβ-Wt assembled predominantly into globular oligomers, which first appeared after 10 min and continuously increased in number during a 2-h incubation period (Fig. 1*A*, *upper panel* and Movie S1 in Supplemental Data). At the same concentration, Aβ-Arctic assembled into short rod-shaped protofibrils in less than 1 h (Fig. 1*A*, *lower panel* and Movie S2 in Supplemental Data), in agreement with previous reports that the Arctic mutation accelerates the formation of Aβ protofibrils (29–32). The globular Aβ-Wt oligomers were 4–5 nm in height, mobile on mica, and coalesced into extended aggregates with segmented morphologies and

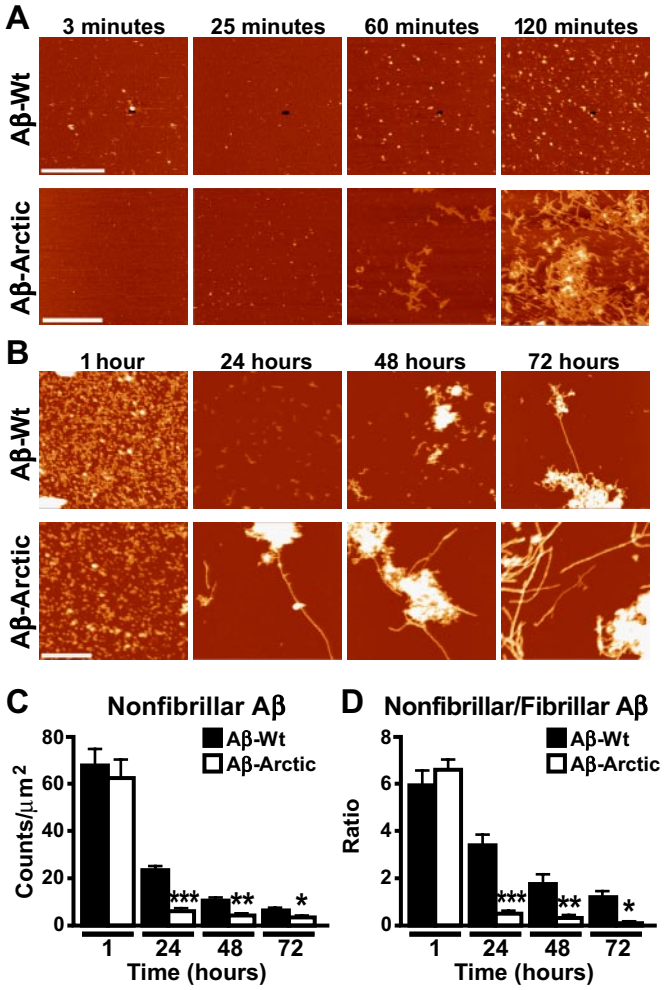

FIGURE 1. **The Arctic mutation increases fibril formation and decreases the nonfibrillar/fibrillar Aβ1–42 ratio *in vitro*.** *A* and *B*, self-assembly of synthetic Aβ-Wt or Aβ-Arctic peptides was monitored by AFM under *in situ* (*A*) or *ex situ* (*B*) cell-free conditions. Color brightness corresponds to relative aggregate height. *A*, freshly prepared monomer solutions (62.5 μM in phosphate-buffered saline) were injected at $t = 0$ directly into the liquid cell of the AFM and imaged continuously (see Movies S1 and S2 in Supplemental Data). As early as 60 min, Aβ-Arctic formed extended aggregates distinctly different from the globular Aβ-Wt aggregates. *B*, monomer solutions (20.8 μM in phosphate-buffered saline) were incubated in tubes at 37 °C with agitation, and then imaged by AFM at the times indicated. After 1 h of incubation, both solutions contained mostly globular oligomeric Aβ. At 24 h, Aβ-Wt was predominately nonfibrillar, and Aβ-Arctic had mature fibril morphologies and large amorphous aggregates. Fibrils and large amorphous aggregates appeared in the Aβ-Wt samples only after 72 h of incubation. Scale bars represent 1 μm (*A*) and 500 nm (*B*). *C* and *D*, numbers of small nonfibrillar Aβ assemblies (*C*) and ratios of nonfibrillar to fibrillar Aβ assemblies (*D*) at each time were determined from 15 images (9–25 μm^2 each) from three independent *ex situ* experiments. Ratios were calculated from the percent surface area occupied by nonfibrillar *versus* fibrillar Aβ assemblies as defined under "Experimental Procedures." *, $p < 0.05$; **, $p < 0.01$; ***, $p < 0.001$ *versus* Aβ-Wt.

often high curvature (Fig. S1, *A* and *B* in Supplemental Data), consistent with earlier findings (45). In contrast, Aβ-Arctic protofibrils were 4.5–5.5 nm in height, had a more rigid morphology, were often highly branched, and formed highly ordered arrays along the crystallographic lattice of the mica surface (Fig. S1, *C* and *D* in Supplemental Data). Aβ-Arctic protofibrils did not grow from an obvious oligomeric precursor on the mica surface, although we cannot exclude the possibility that these structures may have formed transiently in solution before deposition.

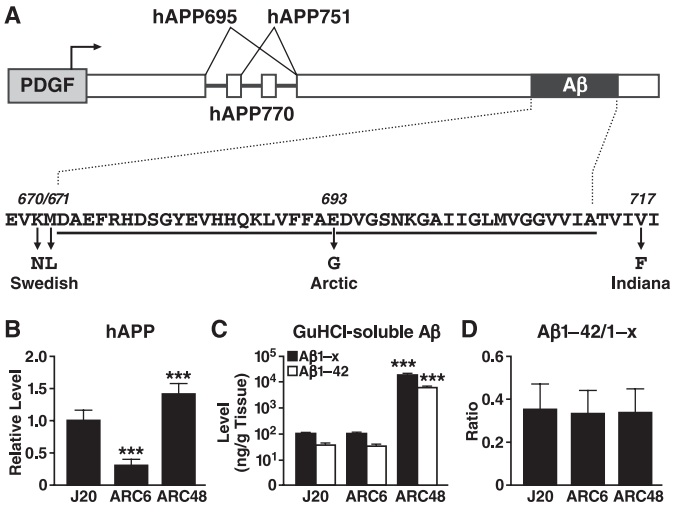

FIGURE 2. **Expression of hAPP and Aβ in transgenic brain.** *A*, diagram of the PDGF-hAPP transgene. Elements are not to scale. The PDGF β-chain promoter directs an alternatively spliced hAPP minigene (67). *B–D*, forebrain lysates of 3–4-month-old mice were analyzed by Western blotting to determine relative levels of hAPP (*B*) or by ELISA to determine levels of guanidine hydrochloride (GuHCl)-soluble Aβ1-x and Aβ1–42 (*C*), and Aβ1–42/Aβ1-x ratios (*D*). Mean hAPP levels in J20 mice were defined as 1.0. $n = 8$–9/group. ***, $p < 0.001$ *versus* J20.

To quantify the levels of various structural assemblies of Aβ that accumulate over longer periods of time, Aβ samples at lower concentration (20.8 μM) were allowed to aggregate in test tubes at 37 °C before *ex situ* analysis by AFM (35). The majority of Aβ-Wt assemblies that appeared within 48 h of incubation were globular oligomers (1–2.5 nm in height) and short rod-shaped protofibrils (3–5 nm in height), whereas elongated fibrils and larger aggregates that were taller than 6 nm in height appeared only after 72 h (Fig. 1*B*, *upper panel* and Fig. S2, *A* and *B* in Supplemental Data). Under the same conditions, Aβ-Arctic remained in small nonfibrillar states at 1 h but had already assembled into fibrils and larger aggregates by 24 h (Fig. 1*B*, *lower panel* and Fig. S2, *C* and *D* in Supplemental Data). These results differ from the original report of the Arctic mutation (29), which concluded that it does not affect the Aβ fibrillization rate. Differences in experimental conditions that may explain this discrepancy include the use of Aβ1–42 instead of Aβ1–40 and of AFM instead of size exclusion chromatography in the current study. Our AFM findings are consistent with other studies demonstrating that the Arctic mutation accelerates fibril formation (30–33, 46). Notably, after 24 h of incubation, samples containing Aβ-Arctic had significantly fewer nonfibrillar assemblies (Fig. 1*C*) and lower ratios of nonfibrillar to fibrillar assemblies than samples containing Aβ-Wt (Fig. 1, *C* and *D*).

*Effects of the Arctic Mutation on Plaque Load and Aβ*56 Levels in Vivo*—To examine the effect of the Arctic mutation on Aβ assembly *in vivo*, we studied three lines of hAPP transgenic mice that produce human Aβ-Wt (line J20) or Aβ-Arctic (lines ARC6 and ARC48) (Fig. 2*A*). The Swedish and Indiana familial AD mutations within hAPP sequences flanking Aβ (Fig. 2*A*) were introduced into all three lines to maximize production of the pathogenic Aβ1–42 species. Because J20 mice carry only these mutations, their transgene-derived Aβ has the sequence of wild-type human Aβ. Because both ARC lines in addition carry the Arctic mutation, which resides in the middle of Aβ, they produce Arctic-mutant human Aβ.

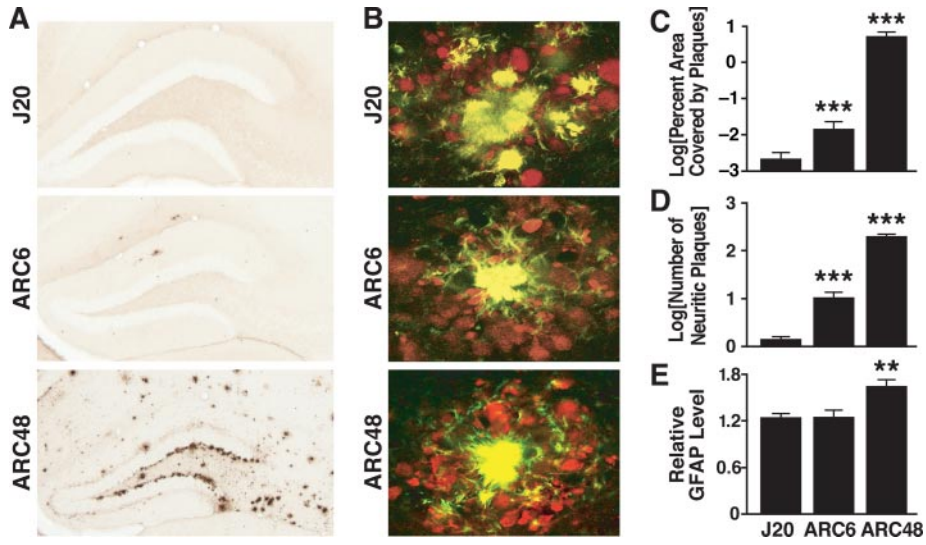

FIGURE 3. **Accelerated plaque formation in ARC lines.** *A–D*, hippocampal plaques were assessed in hAPP mice from lines J20, ARC6, and ARC48 at 3–4 (*A* and *C*) and 10–12 (*B* and *D*) months of age. *A*, Aβ deposits were detected by immunostaining with the 3D6 antibody. *B*, mature plaques were detected by thioflavin-S staining (*green*) and plaque-associated dystrophic neurites with the 8E5 antibody (*red*). *C* and *D*, Plaque loads were determined by measuring the percent area covered by 3D6-immunoreactive Aβ deposits (*C*) and by counting the number of neuritic plaques double-labeled with thioflavin-S and 8E5 (*D*). *E*, levels of reactive astrocytosis in the dentate gyrus of 3–4-month-old mice were determined by densitometric analysis of GFAP immunoreactivity. $n = 8$–10/group. **, $p < 0.01$; ***, $p < 0.001$ *versus* J20.

The levels of hAPP in the forebrain were lower in ARC6 mice and higher in ARC48 mice than in J20 mice (Fig. 2*B*). At 3–4 months of age, levels of guanidine-soluble Aβ1-x and Aβ1–42 in the forebrain were comparable in J20 and ARC6 mice and much higher in ARC48 mice (Fig. 2*C*). The Aβ1–42/Aβ1-x ratios were similar in all three lines (Fig. 2*D*).

An analysis of plaque formation in the hippocampus confirmed and extended our previous observations (34). At 3–4 months, hippocampal Aβ deposition was undetectable or minimal in J20 mice, moderate in ARC6 mice, and prominent in ARC48 mice (Fig. 3, *A* and *C*). Only

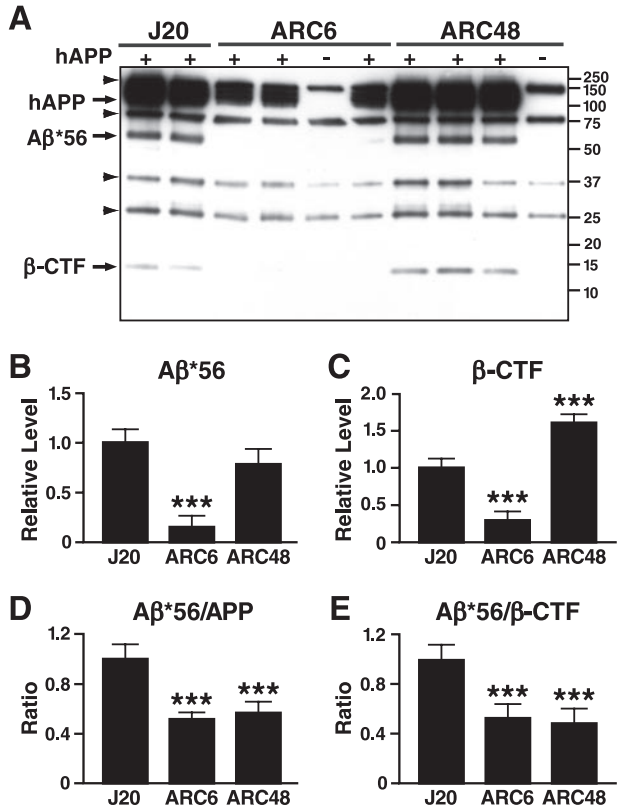

FIGURE 4. **Levels of Aβ*56 and other hAPP products at 3–4 months of age.** *A–E*, Western blot analysis was used to detect APP metabolites and Aβ assemblies in membrane-enriched fractions of forebrain lysates. *A*, representative Western blot probed with the anti-Aβ3-8 antibody 6E10. Identified bands are labeled on the *left* of the blot; *arrowheads* indicate nonspecific signals. *B–E*, densitometry was used to quantify Western blot signals for Aβ*56 (*B*), β-CTF (*C*), Aβ*56/APP (*D*), and Aβ*56/β-CTF ratios (*E*). Mean levels in J20 mice were defined as 1.0. $n = 16–18$/group. ***, $p < 0.001$ *versus* J20.

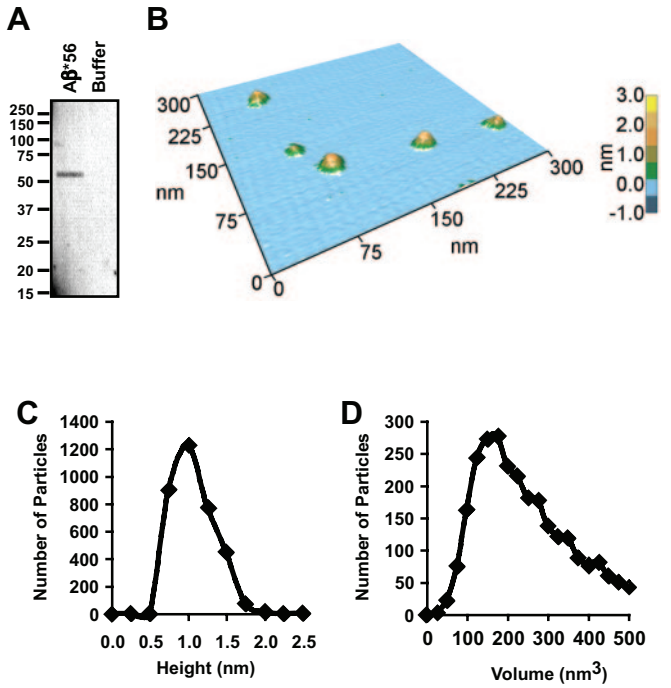

FIGURE 5. ***Ex situ* AFM height image and size distribution of wildtype Aβ*56.** *A*, Western blot analysis (6E10 antibody) of wild-type Aβ*56 purified from RIPA-soluble forebrain lysates of Tg2576 mice by immunoaffinity chromatography and size exclusion chromatography as described (15). *B*, representative 1-μm^2 AFM image of Aβ*56 demonstrating ellipsoidal shapes. *C* and *D*, analysis of 3243 particles in 26 images (5 × 5 μm). The mode of the height was ~1 nm (*C*), and the volume was 125–175 nm^3 (*D*).

ARC48 mice showed reactive astrocytosis (Fig. 3*E*). At 10–12 months, thioflavin-S-positive mature plaques with dystrophic neurites were present in all three lines (Fig. 3*B*) but were much more abundant in the ARC lines than in line J20 (Fig. 3*D*).

Recent studies have identified a specific nonfibrillar Aβ assembly (Aβ*56) in brains of hAPP mice from another line (Tg2576) that was closely linked to memory deficits in these mice and caused memory deficits when infused into the brains of NTG rats (15). Western blot analysis detected a band consistent with Aβ*56 in the membrane-enriched fraction of forebrain lysates from 3–4-month-old hAPP mice (Fig. 4*A*). This fraction also contained full-length hAPP and various APP metabolites, including putative β-secretase-generated C-terminal APP fragments (β-CTF) (Fig. 4*A*). In contrast to their vastly different plaque loads (Fig. 3, *A* and *C*), J20 and ARC48 mice had roughly comparable Aβ*56 levels with a trend toward lower levels in ARC48 mice (Fig. 4*B*). Aβ*56 levels were much lower in the ARC6 line (Fig. 4*B*). In contrast, full-length hAPP (Fig. 2*B*) and β-CTF levels were significantly higher in ARC48 mice than in J20 mice and much lower in ARC6 mice (Fig. 4, *A* and *C*), consistent with previous findings (34). Compared with the J20 line, both ARC lines showed similar decreases in the ratio of Aβ*56 to hAPP (Fig. 4*D*) and the ratio of Aβ*56 to β-CTF (Fig. 4*E*).

Because the morphology of nonfibrillar Aβ assembled *in vivo* has never been examined, we used *ex situ* AFM to image Aβ*56 purified directly from brain tissue of hAPP mice (Fig. 5*A*). Most Aβ*56 particles detected by AFM had a globular ellipsoidal shape (Fig. 5*B*). Size characterization analysis revealed these aggregates to be ~1 nm in height (Fig. 5*C*) and 125–175 nm^3 in volume (Fig. 5*D*), after partial correction for the finite shape and size of the AFM tip. This size is similar to that of the small globular oligomers of synthetic Aβ we identified at early stages in our *in vitro* aggregation experiments (Fig. S2*A* in Supplemental Data).

*Functional Deficits Relate More Closely to Aβ*56 Than to Plaques*—To determine if the increased plaque burden and neuritic dystrophy in ARC mice were associated with more severe behavioral deficits, we compared 3–4-month-old hAPP mice and NTG controls in a Morris water maze. Consistent with previous findings in J20 mice (20) and other hAPP lines overexpressing Aβ-Wt (37), J20 mice required more time than NTG mice to learn to escape to a cued platform that was moved to a different location between sessions, although their performance ultimately reached control levels (Fig. 6*A*). In contrast, ARC6 mice with greater hippocampal plaque loads and even the plaque-laden ARC48 mice had no difficulty learning this task (Fig. 6*A*).

In the spatial component of the water maze test, mice must use extramaze cues to navigate to a platform hidden in a constant location. J20 mice never learned this task as well as NTG controls (Fig. 6*B*), consistent with previous observations (20). ARC6 mice performed as well as NTG controls, but the higher

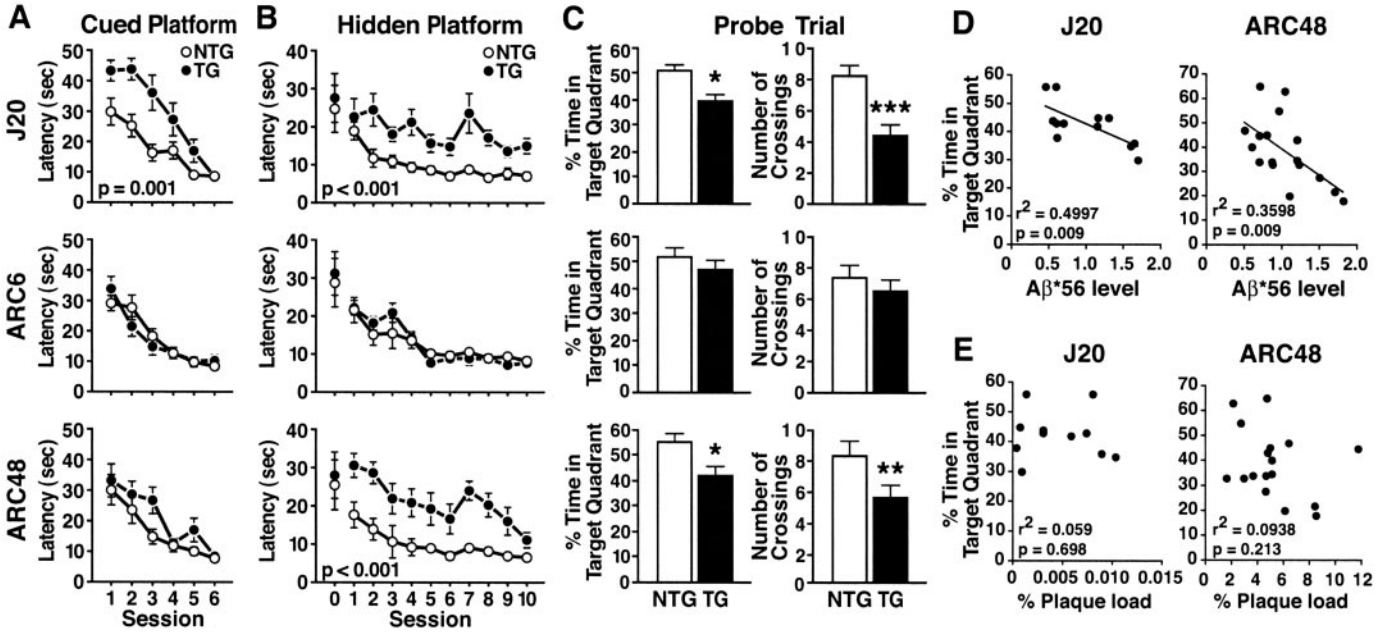

FIGURE 6. **Association between learning/memory deficits and Aβ*56 levels.** *A–C*, Transgenic (*TG*) and nontransgenic (*NTG*) mice from the indicated lines were tested in the Morris water maze at 3–4 months of age. Mice were first trained to locate a cued platform (*A*) and then a hidden platform (*B*). Escape latency (sec) and path length (not shown) were used as measures of learning. The first data point in B(0) indicates performance on the first of three trials in session 1. Subsequent points represent average performance in each session. *C*, mice were tested in a probe trial 16–18 h after the last hidden platform trial. During this test, the platform was removed, and the search patterns of the mice were monitored. $n = 9–13$/group. *, $p < 0.05$; **, $p < 0.01$; ***, $p < 0.001$ *versus* NTG. *D* and *E*, relationship between probe trial performance in the water maze and levels of Aβ*56 (*D*) and plaque load (*E*) at 3–4 months of age. Levels of Aβ*56 in individual mice were normalized to the average levels in transgenic mice from the respective line. $n = 12–18$/group.

expresser ARC48 mice were impaired (Fig. 6*B*). No significant differences were identified in the learning curves in the cued or spatial component of the test between the NTG mice from these three lines (Fig. 6, *A* and *B*).

A day after the last training session, mice were tested in a probe trial during which search patterns were monitored in the absence of a platform. J20 and ARC48 mice showed less preference for the original target location than NTG controls, whereas ARC6 mice had normal spatial memory retention (Fig. 6*C*). In both J20 and ARC48 mice, probe trial deficits correlated with Aβ*56 levels (Fig. 6*D*), but not with plaque loads (Fig. 6*E*) or with hAPP and β-CTF levels (Fig. S3 in Supplemental Data).

Water-maze deficits in J20 mice also correlate well with the depletion of calcium- and synaptic activity-related proteins in granule cells of the dentate gyrus (20, 38, 44). The calcium-binding protein calbindin-D28K and the immediate-early gene product Fos are among the most robust and sensitive of these biomarkers. Compared with NTG controls, calbindin (Fig. 7*A*) and Fos (Fig. 7*B*) levels in the dentate gyrus were significantly reduced in J20 and ARC48 mice, but not in ARC6 mice.

Other Behavioral Alterations and Premature Death—Several lines of hAPP mice expressing high levels of human Aβ-Wt have increased locomotor activity (37), and similar abnormalities have been observed in rats after disruption of input from the entorhinal cortex to the dentate gyrus (41). To look for this behavioral abnormality in our hAPP lines, we used the open field test and the Y maze. In both tests, J20 mice were significantly more active than NTG controls, whereas ARC6 mice were not (Fig. 8, *A* and *B*). ARC48 mice showed a trend toward hyperactivity. J20 mice (38, 39) and other hAPP models (37) also show an abnormal phenotype in the elevated plus maze, which is widely used to assess emotionality (40). In this test, ARC6 mice again behaved normally, whereas J20 mice and ARC48 mice traveled longer distances on the open arms of the maze than NTG controls (Fig. 8*C*). Performance in the open field and plus maze did not correlate with Aβ*56 or β-CTF levels (Fig. S4 in Supplemental Data).

Last, hAPP mice expressing high levels of human Aβ-Wt have an increased incidence of premature death, the cause of which remains unknown (42, 43). Significant premature mortality was evident in lines J20 and ARC48, but not in ARC6 (Fig. 8*D*).

DISCUSSION

These results demonstrate a striking dissociation between plaque formation and functional deficits. ARC6 mice had more plaques than J20 mice but essentially no behavioral deficits. To our knowledge, ARC6 is the first hAPP line to show prominent neuritic plaques but normal learning and memory in the Morris water maze. Furthermore, ARC48 mice had markedly greater plaque loads than J20 mice but comparable or less severe functional deficits (Table S1 in Supplemental Data).

We think that these findings can be explained by differences in Aβ*56 levels and by the kinetic model presented in Fig. 9. Levels of pathogenic oligomers, such as Aβ*56, likely depend on many factors, including hAPP levels, production and degradation of Aβ, and sequestration of Aβ monomers or oligomers into mature fibrils. Although hAPP/Aβ levels in ARC6 mice were not high enough to result in the formation of Aβ*56 or in functional deficits, they were high enough for plaque formation to occur, presumably because of the high fibrillogenic propensity imparted by the Arctic mutation. The effective fibrillization of

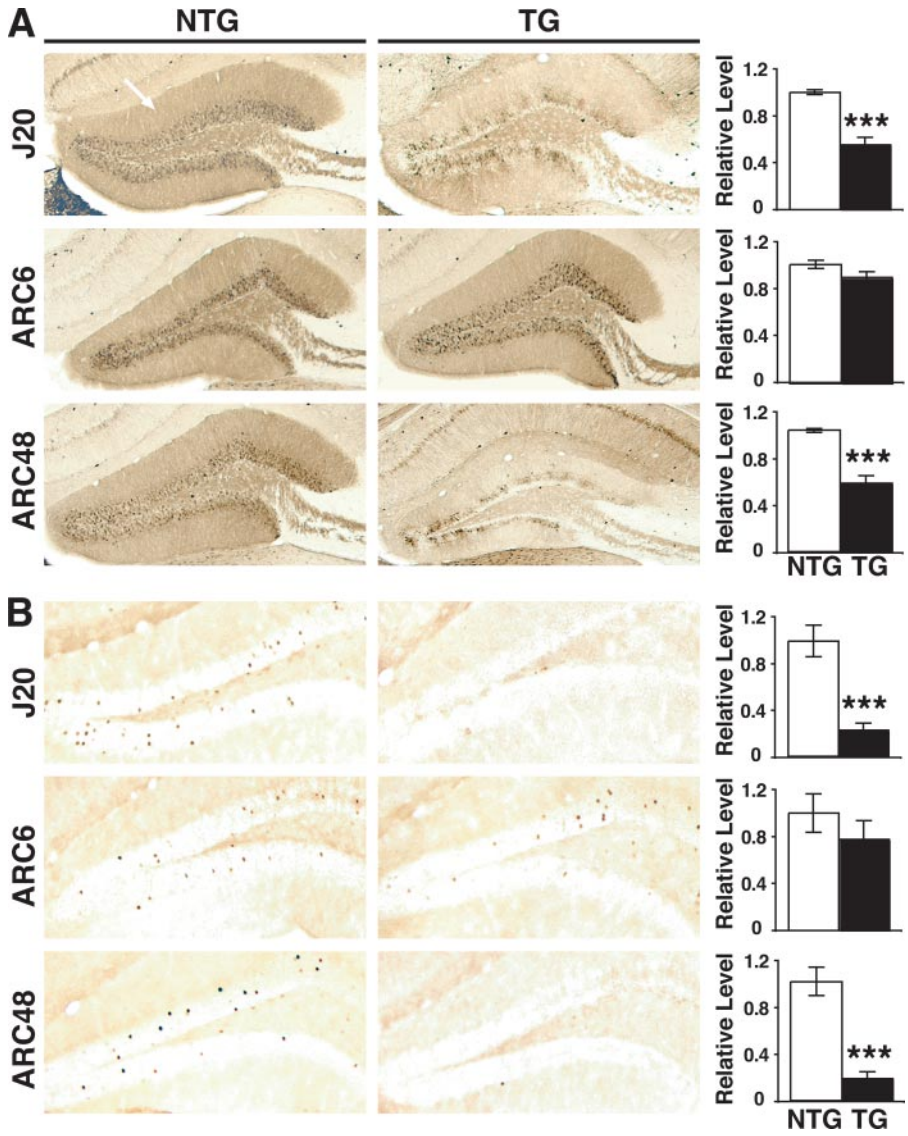

FIGURE 7. **Depletion of synaptic activity-related proteins in the dentate gyrus.** Coronal brain sections of 3–4-month-old mice from the indicated lines were immunostained for calbindin or Fos. *A*, relative calbindin levels were determined by densitometric analysis of the molecular layer (*arrow*) from two sections per mouse. *B*, Fos-positive granule cells in the dentate gyrus were counted in every 10th serial section throughout the rostrocaudal extent of the hippocampus. For both measures, the mean level in NTG mice was defined as 1.0. $n = 9–13$/group. ***, $p < 0.001$ *versus* NTG.

Aβ-Arctic may also explain why Aβ*56/APP ratios were lower in ARC48 than J20 mice. Nevertheless, hAPP/Aβ levels in ARC48 mice were high enough to result in robust levels of Aβ*56 and neuronal dysfunction. In mice overexpressing Aβ-Wt or Aβ-Arctic, behavioral and neuronal deficits were closely related to Aβ*56 levels, but not to plaque loads, consistent with other evidence suggesting that AD-related functional deficits are more likely caused by nonfibrillar Aβ assemblies than by amyloid plaques (1, 15, 16, 19, 47, 48).

Although APP and CTFs are biologically active and can have cytotoxic properties (56–61), their levels did not correlate with the severity of behavioral deficits in our mouse models, making them less likely culprits than nonfibrillar Aβ assemblies, such as Aβ*56. Interestingly, Aβ*56 levels correlated with water-maze deficits but not with activity measurements in the open field and plus maze, suggesting that Aβ*56 may affect learning and memory more than other behavioral domains. In addition, Aβ*56 levels may be higher in brain regions responsible for learning and memory than in brain regions that govern activity in the open field and plus maze. Because available methods are not yet sensitive enough to detect Aβ*56 in very small tissue samples, technological advances will likely be required to assess these possibilities experimentally.

By AFM analysis, Aβ*56 isolated from hAPP mouse brains was ~1 nm in height and 125–175 nm^3 in volume and was similar in size to early-stage synthetic oligomers detected in our AFM analysis but smaller than most synthetic Aβ oligomers and protofibrils reported by others (8, 62, 63). Assuming that the calculated volume of an Aβ monomer folded into a two-stranded β-sheet is ~10 nm^3 (64) and that Aβ*56 is a dodecamer, as suggested by its apparent molecular weight (15), a perfectly packed Aβ*56 should have a volume of ~120 nm^3. Because the finite size of the AFM tip convolutes the lateral dimensions of each particle, resulting in exaggerated volume measurements, we applied geometric methods to partially compensate for this convolution in our quantitative analysis. Because this correction protocol underestimates lateral tip contributions (36), it is not surprising that the Aβ*56 volumes we measured were slightly larger than the theoretical values. Although our results do not exclude the possibility that larger oligomers and protofibrils are also pathogenic, they suggest that small globular oligomers assembled *in vitro* more closely resemble Aβ oligomers that can cause memory deficits *in vivo*.

Because many factors can influence Aβ aggregation, our *in vitro* experiments were performed as close to physiological conditions as possible in regards to temperature, ionic strength, and pH. Because surface chemistry can influence Aβ aggregation during *in situ* AFM imaging (45), all quantitative results were obtained by *ex situ* AFM on Aβ aggregated in solution in the absence of mica. We used mica for *in situ* experiments because Aβ-Wt aggregates that form on mica closely resemble those formed under "free solution" conditions (45). Interestingly, protofibrillar structures formed on mica during *in situ* AFM differed markedly between Aβ-Wt and Aβ-Arctic. As noted in previous studies (45), Aβ aggregation observed by *in*

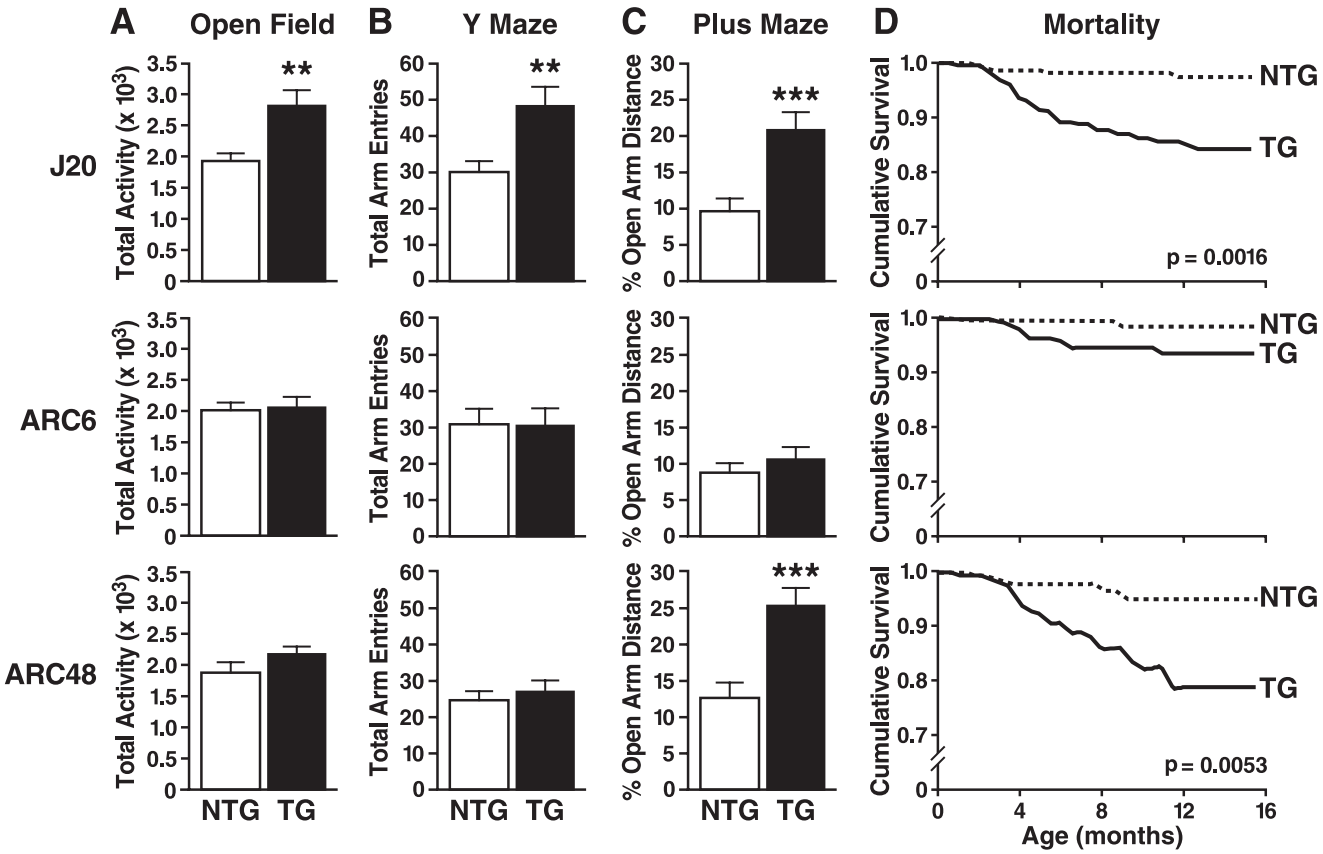

FIGURE 8. **Locomotor activity and premature mortality in hAPP lines.** *A–C*, locomotor activity in mice from the indicated lines was assessed at 3–4 months of age. *A*, in the open field, total activity (beam breaks) was monitored during 15 min of exploration. *B*, in the Y maze, total arm entries were counted for 6 min. *C*, in the elevated plus maze, the percent distance traveled in the open arms relative to the total distance traveled was monitored during 10 min of exploration. $n = 9–13$/group. **, $p < 0.01$; ***, $p < 0.001$ *versus* NTG. *D*, the cumulative proportion of survival in 220–310 mice per genotype (440–610 mice per line) was recorded between birth and 16 months of age.

situ AFM is highly dependent on the surface chemistry of the substrate. When exposed to aqueous solutions, the surface of mica bears a negative charge, similar to the surface of cell membranes containing anionic phospholipids. The E22G mutation reduces the net charge of Aβ-Arctic compared with Aβ-Wt, which may result in differential interactions of these peptides with anionic surfaces both *in vitro* and *in vivo*.

A number of comments are in order about the relation of our models to human carriers of the Arctic mutation. First and foremost, our ARC48 line demonstrates that Aβ-Arctic can result in the formation of Aβ*56 as well as in the development of cognitive deficits, which is perfectly consistent with the fact that the Arctic mutation causes familial AD in humans. However, human carriers are typically heterozygotes, expressing both Aβ-Wt and Aβ-Arctic. *In vitro*, nonfibrillar Aβ assemblies persist longer and fibril formation occurs later in mixtures of Aβ-Arctic and Aβ-Wt than in samples containing only Aβ-Arctic (30). Although our ARC lines express wild-type murine APP and Aβ, the only human Aβ produced at high levels in their brains is Aβ-Arctic. In addition, people with the Arctic mutation do not have the Swedish and Indiana mutations, which were incorporated in our ARC lines to increase Aβ1–42 production to levels that are readily detectable and likely to yield pathological alterations within a short time. Because Aβ1–42 is more fibrillogenic than Aβ1–40 (25, 65), the high Aβ1–42/Aβ1-x ratios in our ARC lines may have synergized with the fibrillogenic effects of the Arctic mutation. Furthermore, wild-type Aβ1–40 can prevent aggregation and deposition of Aβ1–42 (18, 26, 27). Thus, the presence of Aβ-Wt, in combination with potentially lower Aβ1–42/Aβ1–40 ratios, in the brains of human carriers may promote the accumulation of nonfibrillar Aβ assemblies and worsen neurological deficits relative to our ARC models.

Because the pathogenicity of Aβ is linked so tightly to its assembly state, it is difficult, if not impossible, to determine if the Arctic mutation affects the pathogenicity of Aβ independently of its effects on Aβ assembly. How one interprets our results in this regard depends on the relative pathogenic impact of oligomers *versus* plaques. If plaques were the main cause of functional deficits, the comparable levels of deficits in lines J20 and ARC48 would suggest that plaques containing Aβ-Arctic are much less pathogenic than those containing Aβ-Wt, as the plaque burden was so much greater in the ARC48 line. If oligomers are the main cause of functional deficits, the comparable levels of Aβ*56 and of behavioral and neuronal deficits in lines J20 and ARC48 suggest that Aβ*56 containing Aβ-Arctic or Aβ-Wt are equally pathogenic. Because J20 mice develop functional deficits before plaque formation, we favor the latter conclusion.

In some *in vitro* studies (31, 46, 66), but not others (62, 68), Aβ-Arctic appeared to be more toxic than Aβ-Wt. We find it difficult to relate these findings to our results in transgenic

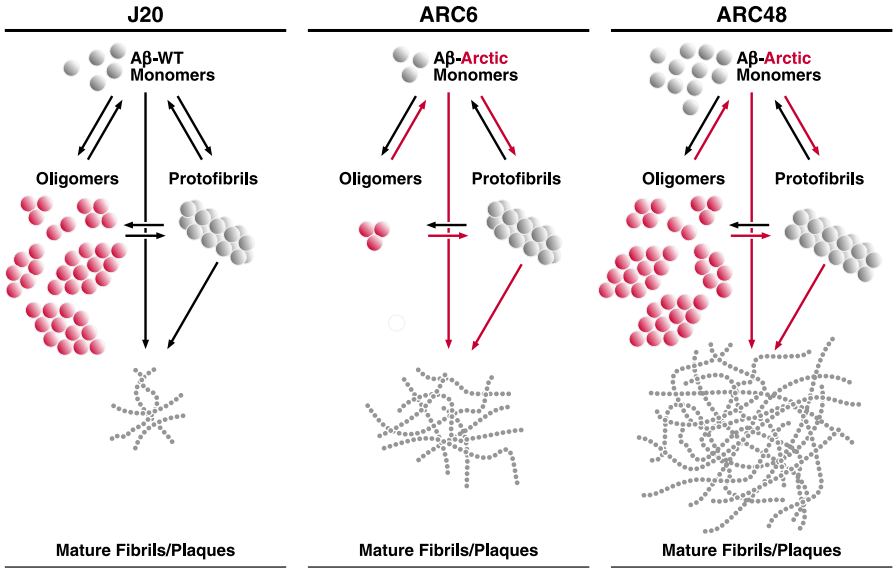

FIGURE 9. **Hypothetical relationship between different Aβ assemblies and neuronal deficits.** The numbers of Aβ monomers at the top roughly correspond to the levels of soluble Aβ detected in the indicated lines at 2–4 weeks of age, when none of them has amyloid deposits (34). Aβ monomers can aggregate into oligomers or protofibrils. However, it is not clear if oligomerization is an intermediate step in the formation of protofibrils and fibrils (*on pathway*) or the end point of an alternative assembly process (*off pathway*). Aβ monomers may also be added directly to growing fibrils without traversing an oligomeric or protofibrillar stage. It is unknown if, under natural conditions, oligomers, protofibrils, or fibrils ever spontaneously dissociate after they have formed. Aβ oligomers are more closely related to neuronal dysfunction and cognitive deficits than fibrils and plaques. If particularly pathogenic oligomers are not on the pathway to fibril formation, accelerating the formation of protofibrils and fibrils may divert a potentially limiting pool of monomers away from oligomer formation. If oligomers are on pathway, accelerating the formation of protofibrils and fibrils may sequester them more rapidly into higher order structures. In either case, the result would be a decrease in the bioactive pool of oligomeric Aβ assemblies. At low monomer levels (as in line ARC6), steady-state levels of oligomers may be too low to elicit functional deficits. At high monomer levels (as in lines ARC48 and J20), steady-state levels of oligomers may reach a critical threshold at which neuronal function becomes impaired, independently of whether Aβ carries the Arctic mutation or not.

mice, because synthetic Aβ preparations with different assembly states were used in the *in vitro* studies, and synthetic Aβ assemblies differ from *in vivo*-generated Aβ assemblies in biological activity even in tissue culture models (69). What is more, the formation of Aβ*56 in brain tissues is age-dependent, and this Aβ assembly does not appear to occur even in primary cortical cultures (15).

We detected Aβ*56 in both the membrane-enriched fraction (Fig. 4*A*) and the extracellular-enriched fraction of forebrain lysates (data not shown). Furthermore, memory deficits in the water maze correlated more strongly with Aβ*56 in the membrane-enriched fraction than in the extracellular-enriched fraction (data not shown). Whether Aβ*56 in the membrane-enriched fraction reflects interactions of this oligomer with the outside or inside of the surface membrane or with membranes of intracellular compartments remains to be determined. While low molecular weight Aβ oligomers have been detected in lysates of APP-expressing CHO cells (7PA2) and primary neurons, Aβ*56 was undetectable in both systems (15), suggesting that this oligomer forms extracellularly.

Although our study was not designed to assess diagnostic procedures or therapeutic interventions, it highlights the dissociation between plaques and neurological deficits, as well as the impact of altering Aβ fibrillization *in vivo*. Both aspects have potentially important clinical implications. There is justifiable excitement in the field about plaque detection with radiopharmaceutical probes in the brains of live patients, an approach that is being included as an outcome measure in an increasing number of clinical trials (70, 71). Notably, diverse factors can alter the aggregation or deposition of Aβ after it is produced (39, 72–76), which could make the relationship between Aβ production and plaque load more complex and less predictable than is desirable from a clinical trials perspective. In addition, the results of the current study suggest that the relationship between Aβ levels and cognitive decline may depend on the balance between fibrillar and nonfibrillar Aβ assemblies, which could be influenced by endogenous factors as well as drug treatments.

Our study also raises some concerns about therapeutic efforts to block or reverse the formation of Aβ fibrils. The risk/benefit ratio of this approach might critically depend on the extent to which it also diminishes the pool of pathogenic Aβ oligomers. Within the obvious constraints of mouse-to-human extrapolations, our data caution against any strategies that decrease Aβ fibrils at the cost of augmenting pathogenic Aβ oligomers. They also raise the possibility that promoting fibril formation in ways that bypass oligomer formation or rapidly sequester oligomers into more inert fibrils might be of therapeutic benefit. Additional studies are needed to further test these hypotheses.

Acknowledgments—We thank J. Weissman for providing access to his AFM; G.-Q. Yu, F. Yan, X. Wang, D. Kim and H. Solanoy for technical assistance; J. Carroll, C. Goodfellow, and T. Roberts for preparation of graphics; G. Howard and S. Ordway for editorial review; and D. McPherson and L. Manuntag for administrative assistance.

REFERENCES

1. Walsh, D. M., and Selkoe, D. J. (2004) *Neuron* **44,** 181–193
2. Tanzi, R., and Bertram, L. (2005) *Cell* **120,** 545–555
3. Skovronsky, D. M., Lee, V. M.-Y., and Trojanowski, J. Q. (2006) *Annu. Rev. Pathol. Mech. Dis.* **1,** 151–170
4. Hebert, L., Scherr, P., Bienias, J., Bennett, D., and Evans, D. (2003) *Arch. Neurol.* **60,** 1119–1122
5. Ferri, C. P., Prince, M., Brayne, C., Brodaty, H., Fratiglioni, L., Ganguli, M., Hall, K., Hasegawa, K., Hendrie, H., Huang, Y., Jorm, A., Mathers, C., Menezes, P. R., Rimmer, E., and Scazufca, M. (2005) *Lancet* **366,** 2112–2117
6. Lleó, A., Greenberg, S. M., and Growdon, J. H. (2006) *Annu. Rev. Med.* **57,** 513–533
7. Roher, A. E., Chaney, M. O., Kuo, Y.-M., Webster, S. D., Stine, W. B., Haverkamp, L. J., Woods, A. S., Cotter, R. J., Tuohy, J. M., Krafft, G. A., Bonnell, B. S., and Emmerling, M. R. (1996) *J. Biol. Chem.* **271,** 20631–20635

8. Lambert, M. P., Barlow, A. K., Chromy, B. A., Edwards, C., Freed, R., Liosatos, M., Morgan, T. E., Rozovsky, I., Trommer, B., Viola, K. L., Wals, P., Zhang, C., Finch, C. E., Krafft, G. A., and Klein, W. L. (1998) *Proc. Natl. Acad. Sci. U. S. A.* **95,** 6448–6453
9. Hartley, D. M., Walsh, D. M., Ye, C. P., Diehl, T., Vasquez, S., Vassilev, P. M., Teplow, D. B., and Selkoe, D. J. (1999) *J. Neurosci.* **19,** 8876–8884
10. Walsh, D. M., Tseng, B. P., Rydel, R. E., Podlisny, M. B., and Selkoe, D. J. (2000) *Biochemistry* **39,** 10831–10839
11. Bitan, G., Lomakin, A., and Teplow, D. B. (2001) *J. Biol. Chem.* **276,** 35176–35184
12. Lashuel, H. A., Hartley, D., Petre, B. M., Walz, T., and Lansbury, P. T., Jr. (2002) *Nature* **418,** 291
13. Hoshi, M., Sato, M., Matsumoto, S., Noguchi, A., Yasutake, K., Yoshida, N., and Sato, K. (2003) *Proc. Natl. Acad. Sci. U. S. A.* **100,** 6370–6375
14. Barghorn, S., Nimmrich, V., Striebinger, A., Krantz, C., Keller, P., Janson, B., Bahr, M., Schmidt, M., Bitner, R. S., Harlan, J., Barlow, E., Ebert, U., and Hillen, H. (2005) *J. Neurochem.* **95,** 834–847
15. Lesné, S., MT, K., Kotilinek, L., Kayed, R., Glabe, C. G., Yang, A., Gallagher, M., and Ashe, K. H. (2006) *Nature* **440,** 352–357
16. Hsia, A., Masliah, E., McConlogue, L., Yu, G., Tatsuno, G., Hu, K., Kholodenko, D., Malenka, R. C., Nicoll, R. A., and Mucke, L. (1999) *Proc. Natl. Acad. Sci. U. S. A.* **96,** 3228–3233
17. Holcomb, L. A., Gordon, M. N., Jantzen, P., Hsiao, K., Duff, K., and Morgan, D. (1999) *Behav. Genet.* **29,** 177–185
18. Mucke, L., Masliah, E., Yu, G.-Q., Mallory, M., Rockenstein, E. M., Tatsuno, G., Hu, K., Kholodenko, D., Johnson-Wood, K., and McConlogue, L. (2000) *J. Neurosci.* **20,** 4050–4058
19. Westerman, M. A., Cooper-Blacketer, D., Mariash, A., Kotilinek, L., Kawarabayashi, T., Younkin, L. H., Carlson, G. A., Younkin, S. G., and Ashe, K. H. (2002) *J. Neurosci.* **22,** 1858–1867
20. Palop, J. J., Jones, B., Kekonius, L., Chin, J., Yu, G.-Q., Raber, J., Masliah, E., and Mucke, L. (2003) *Proc. Natl. Acad. Sci. U. S. A.* **100,** 9572–9577
21. Cummings, B. J., Pike, C. J., Shankle, R., and Cotman, C. W. (1996) *Neurobiol. Aging* **17,** 921–933
22. Knowles, R. B., Gomez-Isla, T., and Hyman, B. T. (1998) *J. Neuropathol. Exp. Neurol.* **57,** 1122–1130
23. Tsai, J., Grutzendler, J., Duff, K., and Gan, W. B. (2004) *Nat. Neurosci.* **7,** 1181–1183
24. Stern, E. A., Bacskai, B. J., Hickey, G. A., Attenello, F. J., Lombardo, J. A., and Hyman, B. T. (2004) *J. Neurosci.* **24,** 4535–4540
25. Younkin, S. G. (1995) *Ann. Neurol.* **37,** 287–288
26. Snyder, S. W., Ladror, U. S., Wade, W. S., Wang, G. T., Barrett, L. W., Matayoshi, E. D., Huffaker, H. J., Kraft, G. A., and Holzman, T. F. (1994) *Biophys. J.* **67,** 1216–1228
27. Kim, J., Onstead, L., Randle, S., Price, R., Smithson, L., Zwizinski, C., Dickson, D. W., Golde, T., and McGowan, E. (2007) *J. Neurosci.* **27,** 627–633
28. Chiti, F., Stefani, M., Taddei, N., Ramponi, G., and Dobson, C. M. (2003) *Nature* **424,** 805–808
29. Nilsberth, C., Westlind-Danielsson, A., Eckman, C. B., Condron, M. M., Axelman, K., Forsell, C., Stenh, C., Luthman, J., Teplow, D. B., Younkin, S. G., Naslund, J., and Lannfelt, L. (2001) *Nat. Neurosci.* **4,** 887–893
30. Lashuel, H. A., Hartley, D. M., Petre, B. M., Wall, J. S., Simon, M. N., Walz, T., Lansbury, J., and Peter, T. (2003) *J. Mol. Biol.* **332,** 795–808
31. Murakami, K., Irie, K., Morimoto, A., Ohigashi, H., Shindo, M., Nagao, M., Shimizu, T., and Shirasawa, T. (2003) *J. Biol. Chem.* **278,** 46179–46187
32. Johansson, A.-S., Berglind-Dehlin, F., Karlsson, G., Edwards, K., Gellerfors, P., and Lannfelt, L. (2006) *FEBS J.* **273,** 2618–2630
33. Hori, Y., Hashimoto, T., Wakutani, Y., Urakami, K., Nakashima, K., Condron, M. M., Tsubuki, S., Saido, T. C., Teplow, D. B., and Iwatsubo, T. (2006) *J. Biol. Chem.* **282,** 4916–4923
34. Cheng, I., Palop, J., Esposito, L., Bien-Ly, N., Yan, F., and Mucke, L. (2004) *Nat. Med.* **10,** 1190–1192
35. Legleiter, J., Czilli, D. L., Gitter, B., DeMattos, R. B., Holtzman, D. M., and Kowalewski, T. (2004) *J. Mol. Biol.* **335,** 997–1006
36. Legleiter, J., DeMattos, R. B., Holtzman, D. M., and Kowalewski, T. (2004) *J. Colloid Interface Sci.* **278,** 96–106
37. Kobayashi, D. T., and Chen, K. S. (2005) *Genes Brain and Behav.* **4,** 173–196
38. Chin, J., Palop, J. J., Puoliväli, J., Massaro, C., Bien-Ly, N., Gerstein, H., Scearce-Levie, K., Masliah, E., and Mucke, L. (2005) *J. Neurosci.* **25,** 9694–9703
39. Esposito, L., Raber, J., Kekonius, L., Fan, Y., Yu, G.-Q., Bien-Ly, N., Puoliväli, J., Scearce-Levie, K., Masliah, E., and Mucke, L. (2006) *J. Neurosci.* **26,** 5167–5179
40. Belzung, C., and Griebel, G. (2001) *Behav. Brain Res.* **125,** 141–149
41. Steward, O., Loesche, J., and Horton, W. C. (1977) *Brain Res. Bull.* **2,** 41–48
42. Hsiao, K. K., Borchelt, D. R., Olson, K., Johannsdottir, R., Kitt, C., Yunis, W., Xu, S., Eckman, C., Younkin, S., Price, D., Iadecola, C., Clark, H. B., and Carlson, G. (1995) *Neuron* **15,** 1203–1218
43. Chin, J., Palop, J. J., Yu, G.-Q., Kojima, N., Masliah, E., and Mucke, L. (2004) *J. Neurosci.* **24,** 4692–4697
44. Palop, J. J., Chin, J., Bien-Ly, N., Massaro, C., Yeung, B. Z., Yu, G.-Q., and Mucke, L. (2005) *J. Neurosci.* **25,** 9686–9693
45. Kowalewski, T., and Holtzman, D. M. (1999) *Proc. Natl. Acad. Sci. U. S. A.* **96,** 3688–3693
46. Whalen, B. M., Selkoe, D. J., and Hartley, D. M. (2005) *Neurobiol. Dis.* **20,** 254–266
47. Holcomb, L., Gordon, M. N., McGowan, E., Yu, X., Benkovic, S., Jantzen, P., Wright, K., Saad, I., Mueller, R., Morgan, D., Sanders, S., Zehr, C., O'Campo, K., Hardy, J., Prada, C. M., Eckman, C., Younkin, S., Hsiao, K., and Duff, K. (1998) *Nat. Med.* **4,** 97–100
48. Klein, W. L., Krafft, G. A., and Finch, C. E. (2001) *Trends Neurosci.* **24,** 219–224
49. Deleted in proof.
50. Deleted in proof.
51. Deleted in proof.
52. Deleted in proof.
53. Deleted in proof.
54. Deleted in proof.
55. Deleted in proof.
56. Rockenstein, E., Mante, M., Alford, M., Adame, A., Crews, L., Hashimoto, M., Esposito, L., Mucke, L., and Masliah, E. (2005) *J. Biol. Chem.* **280,** 32957–32967
57. Kerr, M. L., and Small, D. H. (2005) *J. Neurosci. Res.* **80,** 151–159
58. Galvan, V., Gorostiza, O. F., Banwait, S., Ataie, M., Logvinova, A. V., Sitaraman, S., Carlson, E., Sagi, S. A., Chevallier, N., Jin, K., Greenberg, D. A., and Bredesen, D. E. (2006) *Proc. Natl. Acad. Sci. U. S. A.* **103,** 7130–7135
59. Zheng, H., and Koo, E. H. (2006) *Mol. Neurodegener.* **1,** 5
60. Lee, K. W., Im, J. Y., Song, J. S., Lee, S. H., Lee, H. J., Ha, H. Y., Koh, J. Y., Gwag, B. J., Yang, S. D., Paik, S. G., and Han, P. L. (2006) *Neurobiol. Dis.* **22,** 10–24
61. Neve, R. L., and McPhie, D. L. (2007) *Biochim. Biophys. Acta* **1772,** 430–437
62. Dahlgren, K. N., Manelli, A. M., Stine, W. B., Jr., Baker, L. K., Krafft, G. A., and LaDu, M. J. (2002) *J. Biol. Chem.* **277,** 32046–32053
63. Harper, J. D., and Lansbury, P. T. J. (1997) *Annu. Rev. Biochem.* **66,** 385–407
64. Yang, D. S., Yip, C. M., Huang, T. H. J., Chakrabartty, A., and Fraser, P. E. (1999) *J. Biol. Chem.* **274,** 32970–32974
65. Burdick, D., Soreghan, B., Kwon, M., Kosmoski, J., Knauer, M., Henschen, A., Yates, J., Cotman, C., and Glabe, C. (1992) *J. Biol. Chem.* **267,** 546–554
66. Klyubin, I., Walsh, D. M., Cullen, W. K., Fadeeva, J. V., Anwyl, R., Selkoe, D. J., and Rowan, M. J. (2004) *Eur. J. Neurosci.* **19,** 2839–2846
67. Rockenstein, E. M., McConlogue, L., Tan, H., Gordon, M., Power, M., Masliah, E., and Mucke, L. (1995) *J. Biol. Chem.* **270,** 28257–28267
68. Ji, Z. S., Mullendorff, K., Cheng, I. H., Miranda, R. D., Huang, Y., and Mahley, R. W. (2006) *J. Biol. Chem.* **281,** 2683–2692
69. Wang, Q., Walsh, D. M., Rowan, M. J., Selkoe, D. J., and Anwyl, R. (2004) *J. Neurosci.* **24,** 3370–3378
70. Klunk, W. E., Engler, H., Nordberg, A., Wang, Y., Blomqvist, G., Holt, D. P., Bergstrom, M., Savitcheva, I., Huang, G. F., Estrada, S., Ausen, B., Debnath, M. L., Barletta, J., Price, J. C., Sandell, J., Lopresti, B. J., Wall, A., Koivisto, P., Antoni, G., Mathis, C. A., and Langstrom, B. (2004) *Ann. Neurol.* **55,** 306–319

71. Buckner, R. L., Snyder, A. Z., Shannon, B. J., LaRossa, G., Sachs, R., Fotenos, A. F., Sheline, Y. I., Klunk, W. E., Mathis, C. A., Morris, J. C., and Mintun, M. A. (2005) *J. Neurosci.* **25,** 7709–7717
72. Mucke, L., Yu, G.-Q., McConlogue, L., Rockenstein, E. M., Abraham, C. R., and Masliah, E. (2000) *Am. J. Pathol.* **157,** 2003–2010
73. Wyss-Coray, T., Lin, C., Yan, F., Yu, G.-Q., Rohde, M., McConlogue, L., Masliah, E., and Mucke, L. (2001) *Nat. Med.* **7,** 612–618
74. Cherny, R. A., Atwood, C. S., Xilinas, M. E., Gray, D. N., Jones, W. D., McLean, C. A., Barnham, K. J., Volitakis, I., Fraser, F. W., Kim, Y. S., Huang, X. D., Goldstein, L. E., Moir, R. D., Lim, J. T., Beyreuther, K., Zheng, H., Tanzi, R. E., Masters, C. L., and Bush, A. I. (2001) *Neuron* **30,** 665–676
75. Fagan, A. M., Watson, M., Parsadanian, M., Bales, K. R., Paul, S. M., and Holtzman, D. M. (2002) *Neurobiol. Dis.* **9,** 305–318
76. DeMattos, R. B., Cirrito, J. R., Parsadanian, M., May, P. C., O'Dell, M. A., Taylor, J. W., Harmony, J. A. K., Aronow, B. J., Bales, K. R., Paul, S. M., and Holtzman, D. M. (2004) *Neuron* **41,** 193–202